A Novel Grid-Connected PV System Based on MMC to Get the Maximum Power Under Partial Shading Conditions

Fei Rong, Xichang Gong, and Shoudao Huang, *Member, IEEE*

***Abstract*—In the case of partial shading, the output power of the unshaded PV modules will be decreased by the influence of the shaded PV modules in one branch. In order to solve this problem, this paper proposes a novel topology for a PV power generation system by connecting a PV module to the capacitor in each submodule of a modular multilevel converter parallel. As partial shading occurs, the maximum power can be extracted by regulating the capacitor voltage to the maximum power point voltage. With this proposed topology, the maximum power tracking controller, the redundancy module controller, the voltage stability controller, and the grid-connected controller are studied. Simulation and experiment results show that comparing to the traditional topology, the proposed topology can greatly improve the output power of the PV system under the conditions of partial shading and features with low-voltage stress and high efficiency.**

***Index Terms*—Grid-connected, MMC, partial shading, photovoltaic (PV) power generation system, redundancy control.**

I. Introduction

In a photovoltaic (PV) plant, dozens of PV modules are usually connected in series to improve the terminal voltage. As a result, the current of the series branch will decrease significantly under partial shading conditions [1], [2], which will cause the unshaded PV modules unable to work at their maximum power points (MPP), and further reduce the power delivered to the grid [3]. Qahouq and Yuncong Jiang [4] present a method, which splits the long PV string to several short PV strings and designs a boost converter for each to increase the energy harvested from the PV module. However, as the number of short strings increases, the size and cost of the boost converter will increase significantly. A high-voltage gain dc–dc converter is designed in [5], the proposed converter may reduce the power loss of the converter, but have no effect on the power loss caused by partial shading. Acciari *et al.* connect a bypass diode in parallel with every PV module. By this way, the shaded PV modules can be bypassed under partial shading conditions, enabling the unshaded PV modules to work at their MPPs. However, the output ability of the shaded PV modules is sacrificed. Furthermore, the existing multipeak points in the power–voltage (*P–V*) characteristic curve of the series branch may cause the failure of the global maximum power point tracking (MPPT) [8].

In order to improve the output power of PV array under partial shading conditions, Bastidas-Rodriguez *et al.* [9]–[16] investigate different methods of searching the global MPP on the multipeak *P–V* curve. The Futoshiki puzzle pattern for the arrangement of the modules of a PV array under partial shading conditions is studied in [17]. By this way, the shadow is dispersed into the whole PV array to a certain extent and the power loss is reduced. A method of changing the structure of PV array under partial shading to get more power is proposed in [18]. Unfortunately, both the methods introduced in [17] and [18] need a lot of switches which will cause the structure complex. Zengin *et al.* [19] disconnects the PV array from the load for a negligibly short period of time and connects it to an external capacitor in the case of partial shading. During the charging time of the capacitor, the global MPP could be found by a special circuit which will result in an extra cost.

Abdalla *et al.* [20] design a micro-PV inverter for every PV module. It has several advantages such as no mismatch of losses and easy to realize, but the application of a large number of inverters lead to extra power losses and costs. A diode clamping interconnection topology is described in [21] and [22] to realize independent voltage control for each PV module under partial shading conditions, but the structure and control system will become very complex when the number of PV modules is big. In [23], the complexity of the control method and the output efficiency of the PV system are studied by dividing the PV modules into two groups, which is similar to a three-level structure. In other words, the control complexity is reduced at the cost of lowering the output efficiency. Rani *et al.* [24]–[26] study the effect of different connection manners of PV modules and conclude that the PV modules should be connected in parallel as many as possible. Lavado Villa *et al.* [27] compare four topologies, i.e., SP, BL, TCT, and HC, and points out that the shaded PV modules should be connected in parallel and then be connected to the unshaded PV modules in series. Vengatesh and Edward Rajan [28] investigate the *P–U* characteristics of multicrystal PV modules (connected in series, parallel, and series–parallel configurations), and points out that the PV modules must be connected in parallel under partial shading conditions. Although a method for detecting shadows is proposed in [29],

Manuscript received January 22, 2016; revised March 25, 2016 and June 8, 2016; accepted July 19, 2016. Date of publication July 27, 2016; date of current version February 11, 2017. Recommended for publication by Associate Editor V. Agarwal.

The authors are with the College of electrical and information engineering, Hunan University, Changsha 410082, China (e-mail: rf_hunu@126.com; 1627335408@qq.com; hsd1962@hnu.edu.cn).

Color versions of one or more of the figures in this paper are available online at http://ieeexplore.ieee.org.

Digital Object Identifier 10.1109/TPEL.2016.2594078

changing the topology of the PV system in real time requires a lot of switches. In [30], the PV modules are grouped by "binary" or "trinary," and then connected to the grid with H bridge converter. Although a higher voltage level could be obtained by this way, some switches have to suffer the high-voltage stress. Ramya and Ramaprabha [31] connect the PV array to the dc side of the MMC directly, and focuses on the design of the *LCL* output filter, whereas Ramya and Ramaprabha [32] connect PV array to the dc side of the MMC by a BOOST circuit. Both the methods improve the power quality under partial shading. In [33] and [34], the PV modules are connected to the MMC cells through the dc/dc converters to obtain high efficiency and power quality, but the number of the dc/dc circuits is extremely huge.

This paper proposes a novel topology for the PV system by connecting a PV module to the capacitor of each submodule (called PM in following) of MMC in parallel. As partial shading occurs, the maximum power could be extracted by regulating each capacitor voltage to the MPP voltage V_{MPP}. The proposed topology could effectively improve the transmission voltage level by connecting the PM modules in series, which may help us to eliminate the step-up transformer and suits for the large PV plant. Because the PV modules are not connected in series directly, the power losses of the unshaded PV modules in the series branch can be eliminated under partial shading conditions. This topology could also achieve the independent MPPT control of PV modules, and solve the multipeak optimization problem of MPPT under partial shading conditions which may occur in the series connection topology.

II. Novel Topology of the PV Power Generation System

A. Novel Topology of the PV System and Its Mathematical Model

The proposed topology of the PV power generation system is shown in Fig. 1. Comparing to the traditional MMC circuit used in the PV system [35], [36], the proposed one removes the long string PV modules connected to the dc side of the MMC, and connects a PV module to the capacitor of each submodule of the MMC in parallel. Because no PV modules are connected in series, the bypass diodes are also removed. When there is partial shading, the maximum power can be extracted by regulating the capacitor voltage in each PM to V_{MPP}.

The voltage of the capacitor in the PM may fluctuate according to the irradiance. Although the voltage fluctuation is insignificant for a single module, it could not be neglected when a large number of PMs are connected in series. Therefore, a redundant module (RM) is designed to compensate the voltage loss.

The one phase equivalent circuit of the novel topology is shown in Fig. 1(b). As seen in Fig. 1(b), the mathematical model of the novel topology can be expressed by

$$\begin{cases} 2U_j = (U_{jn} - U_{jp}) + L\dfrac{d(I_{jn} - I_{jp})}{dt} \\ I_j = I_{jp} - I_{jn} \\ I_{\mathrm{circ},j} = \dfrac{I_{jp} + I_{jn}}{2} \end{cases} \tag{1}$$

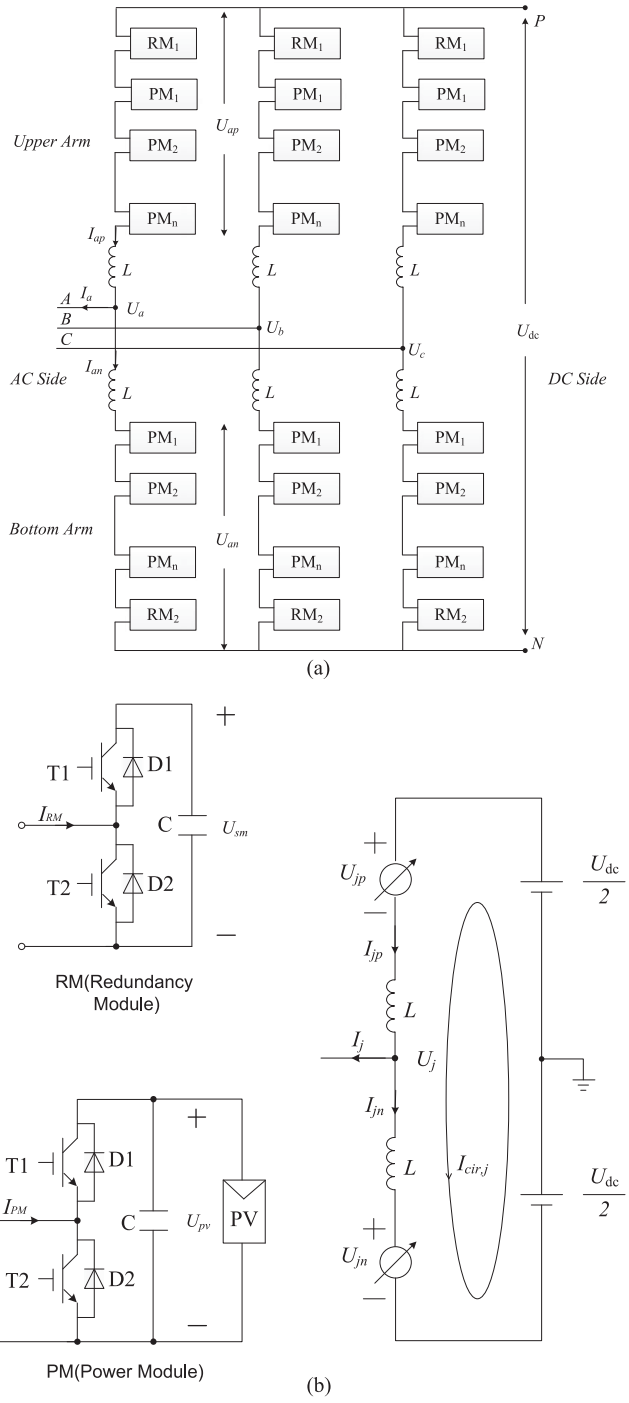

Fig. 1. Novel topology of the PV power generation system. (a) Topology. (b) One-phase equivalent circuit.

where U_j and I_j are the output voltage and output current of phase *j*, respectively $(j = a,b,c)$; U_{jp} is the voltage of upper arm; U_{jn} is the voltage of bottom arm; I_{jp} and I_{jn} are the upper arm's current and the bottom arm's current, respectively; I_{circ}, j is the circulation current; *L* is the buffer inductor.

So

$$\begin{cases} U_j = \frac{1}{2}(U_{jn} - U_{jp}) + \dfrac{1}{2}L\dfrac{dI_j}{dt} \\ U_{dc} = (U_{jn} + U_{jp}) + 2L\dfrac{dI_{\mathrm{circ},j}}{dt} \end{cases} \tag{2}$$

where $U_{\rm dc}$ is the dc-side voltage of the MMC. Let us define

$$\begin{cases} e = \dfrac{1}{2}(U_{jn} - U_{jp}) \\ U_{{\rm circ},j} = L\dfrac{dI_{{\rm circ},j}}{dt} \end{cases}. \tag{3}$$

Then, U_j can be expressed by

$$U_j = e + \frac{1}{2}L\frac{dI_j}{dt}. \tag{4}$$

Hence, I_j could be controlled through controlling e at the suitable modulation voltage. Combining (2) and (3) yields (5), which can be looked as the reference voltage expressions of the upper and bottom arms

$$\begin{cases} U_{jp} = \dfrac{1}{2}U_{\rm dc} - e - U_{{\rm circ},j} \\ U_{jn} = \dfrac{1}{2}U_{\rm dc} + e - U_{{\rm circ},j} \end{cases}. \tag{5}$$

B. Operation States of PM

The operation states of PM are summarized as follows.

State I: T1 is switched ON and T2 is switched OFF, the terminal voltage of PM equals to the capacitor voltage $U_{\rm PV}$.

State II: T1 is switched OFF and T2 is switched ON, the terminal voltage of PM is 0.

State III: T1 is switched OFF and T2 is switched OFF, the terminal voltage of PM is uncertain.

The PM's capacitor voltages under different operation states are described as follows:

1) *State I:* The variation of the PM's capacitor voltage $\Delta U_{\rm PV}$ can be expressed by (6) under this state.

$$\Delta U_{\rm PV} = \frac{1}{C}\int (i_{\rm PV} - i_{\rm PM})dt \tag{6}$$

where $i_{\rm PV}$ is the output current of the PV module, $i_{\rm PM}$ is the output current of the PM, and C is the value of the capacitor in each PM. If the current $i_{\rm PM}$ flows into the PM from the midpoint, as shown in Fig. 2(a), the capacitor will be charged by $i_{\rm PM}$ and $i_{\rm PV}$. Then, the capacitor voltage $U_{\rm PV}$ will rise quickly. Oppositely, if $i_{\rm PM}$ flows out from the PM, $U_{\rm PV}$ will drop when $i_{\rm PM} > i_{\rm PV}$, as shown in Fig. 2(b), and rise when $i_{\rm PM} < i_{\rm PV}$ as shown in Fig. 2(c).

2) *State II:* $\Delta U_{\rm PV}$ is expressed as below under this state

$$\Delta U_{\rm PV} = \frac{1}{C}\int i_{\rm PV}\,dt. \tag{7}$$

The capacitor is charged by $i_{\rm PV}$, and its voltage $U_{\rm PV}$ rises regardless of the direction of $i_{\rm PM}$, as shown in Fig. 2(d) and (e).

3) *State III:* $\Delta U_{\rm PV}$ is expressed by (8) under this state

$$\Delta U_{\rm PV} = \frac{1}{C}\int (S(i_{\rm PM}) + i_{\rm PV})dt \tag{8}$$

where "S()" is a function of $i'_{\rm PM}$, when $i_{\rm PM} \geq 0$, its output is $i_{\rm PM}$, otherwise, its output is 0.

If $i_{\rm PM}$ flows into the PM, as shown in Fig. 2(f), $U_{\rm PV}$ will be charged by $i_{\rm PM}$ and $i_{\rm PV}$ together. As a result, it will rise quickly. Oppositely, if $i_{\rm PM}$ flows out from the PM, as shown in Fig. 2(g), U_{PV} will also rise because it is charged by i_{PV}.

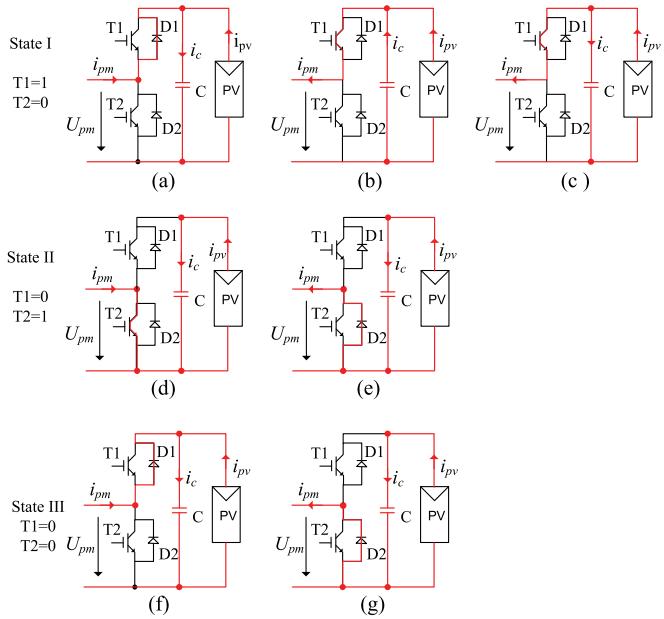

Fig. 2. Working states of PM.

TABLE I
CHANGING TREND OF THE PM'S CAPACITOR VOLTAGE UNDER DIFFERENT WORKING STATES

States	Mode	T1	T2	i_{pm}	U_{pv}
I	(a)	1	0	>0	Ascend
	(b)	1	0	$<0, \lvert ipm \rvert > ipv$	Descend
	(c)	1	0	$<0, \lvert ipm \rvert < ipv$	Ascend
II	(d)	0	1	>0	Ascend
	(e)	0	1	<0	Ascend
III	(f)	0	0	>0	Ascend
	(g)	0	0	<0	Ascend

From the above analyses, the capacitor voltage $U_{\rm PV}$ can be controlled to be the MPP voltage of PV module by choosing suitable working states in according to the direction of $i_{\rm PM}$. Table I shows the relationships of working states, direction of $i_{\rm PM}$, and changing trend of $U_{\rm PV}$. Here, "1" denotes switching on, "0" denotes switching off.

III. CONTROL METHOD OF THE NOVEL PV POWER GENERATION SYSTEM

Taking phase A as an example, the block diagram of the control method is shown in Fig. 3, which is divided into four parts: I) the maximum power tracking controller, 2) the redundancy module controller, 3) the voltage stability controller, and 4) the grid-connected controller. The output of these controllers are $U_{\rm ref1}$,$U_{\rm ref2}$,$U_{\rm ref3}$, and $U_{\rm ref4}$, respectively.

The grid-connected controller gets the main modulation waveform $U_{\rm ref4}$, and its purpose is to achieve the energy delivery from PV module to power grid. The voltage stability controller is used to balance the voltages between phases. The

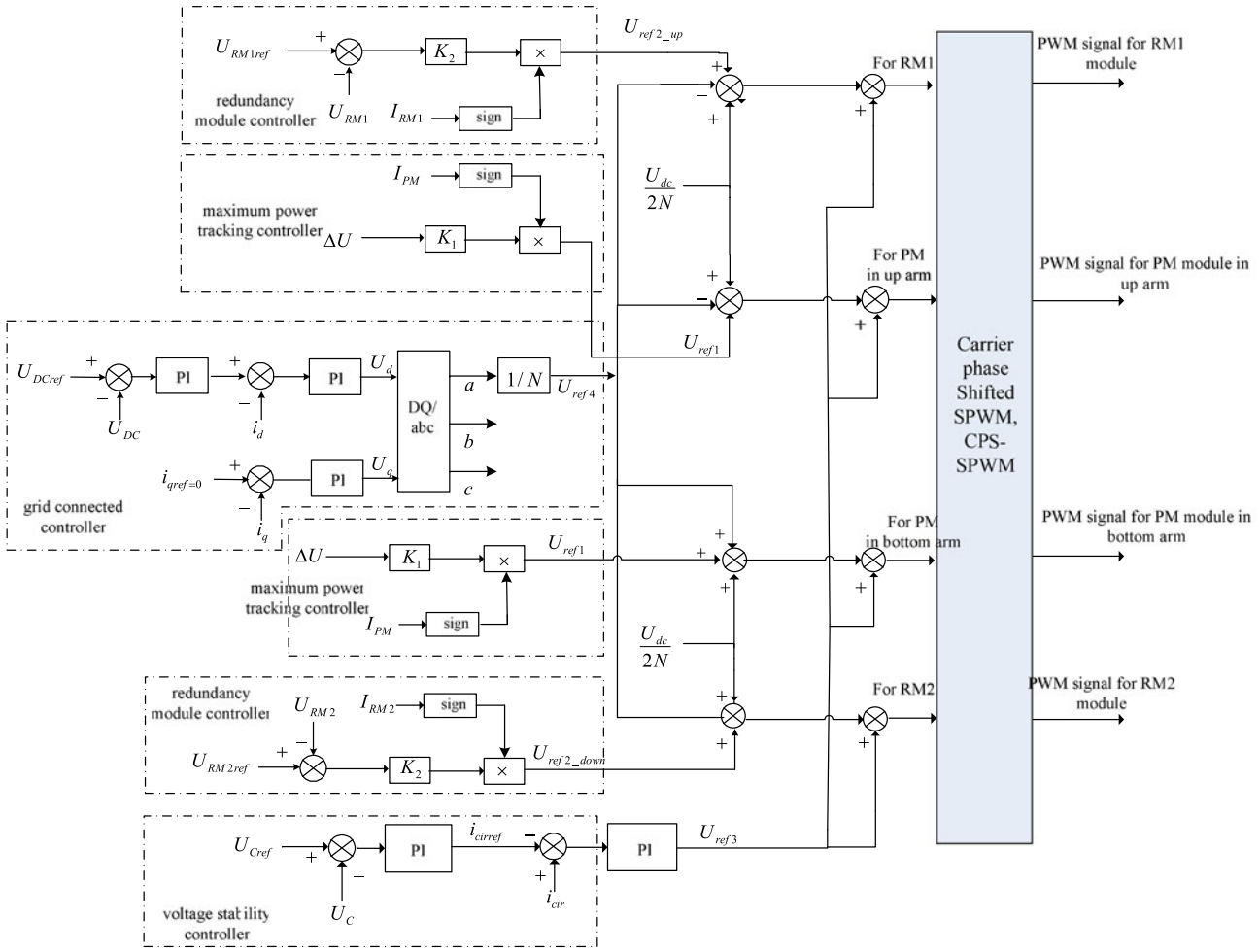

Fig. 3. Block diagram of the control method.

modulation waveform U_{ref3} generated by the voltage stability controller is superimposed on the main modulation waveform, which will change the output power of each phase. Through this adjustment, the voltage balance of phases can be realized. The redundancy module controller is used to regulate the voltage of capacitor in RM. Its output modulation waveform U_{ref2} is superimposed on the main modulation waveform too, which can change the charge and discharge time of the capacitor in RM. The maximum power tracking controller is used to obtain MPP voltage of the PV module. Its working principle is like that of redundancy module controller. When the PV modules work at the MPP, the voltages of capacitors in PMs maybe unequal, but the difference is small, which will have a little influence on the THD of the output current of the topology.

A. Maximum Power Tracking Controller

As shown in Fig. 2, for each PM, the direction of the capacitor current i_C greatly influences the capacitor voltage U_{PV}.When the PM works in State I, $i_C = i_{\mathrm{PM}} + i_{\mathrm{PV}}$, and when the PM works in State II, $i_C = i_{\mathrm{PV}}$.

The P&O method is applied for the maximum power tracking. Assuming ΔU as a perturbation value, if $\Delta U > 0$, the capacitor voltage should rise during the next control period. If $i_{\mathrm{PM}} > 0$, then $i_{\mathrm{PM}} + i_{\mathrm{PV}} > i_{\mathrm{PV}}$, state I will be accordingly selected to accelerate the charging speed for the capacitor. Oppositely, if $i_{\mathrm{PM}} < 0, i_{\mathrm{PM}} + i_{\mathrm{PV}} < i_{\mathrm{PV}}$, State II will be selected to improve the charging speed of the capacitor.

Similarly, if $\Delta U < 0$, the capacitor voltage should decrease during the next control period. If $i_{PM} > 0$, state II will be accordingly selected to decrease surge value; if $i_{\mathrm{PM}} < 0$ and $0 < i_{\mathrm{PM}} + i_{\mathrm{PV}} < i_{\mathrm{PV}}$, state I will be selected to decrease the surge value; if $i_{\mathrm{PM}} < 0$ and $i_{\mathrm{PM}} + i_{\mathrm{PV}} < 0 < i_{\mathrm{PV}}$, state I will be suggested to improve the discharging speed of the capacitor.

As the voltage of the capacitor increases or decreases relying on the direction of arm current, a proportional controller is chosen for the maximum power tracking, which is described by

$$U_{\mathrm{ref1}} = \begin{cases} K_{P1} \cdot \Delta U, & i_{\mathrm{PM}} \geq 0 \\ -K_{P1} \cdot \Delta U, & i_{\mathrm{PM}} < 0 \end{cases} \tag{9}$$

where K_{p1} is the proportional coefficient.

The block diagram of the maximum power tracking controller is shown in Fig. 3. Here, "sign" is a function of i_{PM}, its value will be "1" if $i_{\mathrm{PM}} \geq 0$ and "-1" if $i_{\mathrm{PM}} < 0$.

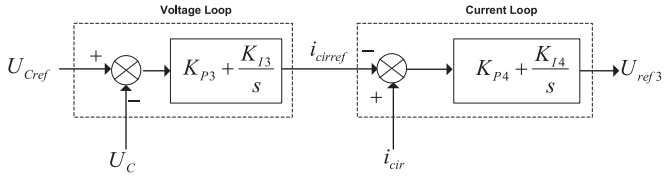

Fig. 4. Block diagram of the voltage stability controller.

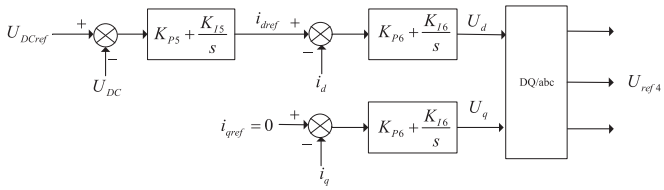

Fig. 5. Block diagram of the grid-connected controller.

B. Redundancy Module Controller

A redundancy module is employed in each bridge arm, as shown in Fig. 1. This module only contributes to compensate the fluctuation voltage of PMs in each bridge arm, and, therefore, improves the reliability of the MMC

In practical application, the sum voltage of all modules in each arm is usually expected to be constant, and its value equals to the reference voltage of the dc-side voltage of MMC U_{DCref}.

As a result, the reference voltage of the redundancy module can be expressed by

$$\begin{cases} U_{\mathrm{RM1ref}} = U_{\mathrm{DCref}} - \sum_{j=1}^{n} U_{\mathrm{up\_}c} \\ U_{\mathrm{RM2ref}} = U_{\mathrm{DCref}} - \sum_{j=1}^{n} U_{\mathrm{down\_}c} \end{cases} \tag{10}$$

where $U_{\mathrm{RM1ref}}, U_{\mathrm{RM2ref}}$ are the reference voltages of the redundancy modules in the upper and bottom arms, respectively. $\sum_{j=1}^{n} U_{\mathrm{up\_}c}$ is the sum voltage of all PMs in upper arm of phase A, and $\sum_{j=1}^{n} U_{\mathrm{down\_}c}$ is the sum voltage of all PMs in the bottom arm of phase A.

Similar to the maximum power control, a proportional controller is chosen for the redundancy modules, which is expressed by

$$U_{\mathrm{ref2\_up}} = \begin{cases} K_{P2} \cdot (U_{\mathrm{RM1ref}} - U_{\mathrm{RM1}}), & i_{\mathrm{RM1}} \geq 0 \\ -K_{P2} \cdot (U_{\mathrm{RM1ref}} - U_{\mathrm{RM1}}), & i_{\mathrm{RM1}} < 0 \end{cases} \tag{11}$$

$$U_{\mathrm{ref2\_down}} = \begin{cases} K_{P2} \cdot (U_{\mathrm{RM2ref}} - U_{\mathrm{RM2}}), & i_{\mathrm{RM2}} \geq 0 \\ -K_{P2} \cdot (U_{\mathrm{RM2ref}} - U_{\mathrm{RM2}}), & i_{\mathrm{RM2}} < 0 \end{cases} \tag{12}$$

where (11) and (12) are used to control the redundancy modules in upper arm and bottom arm, respectively; $U_{\mathrm{RM1}}, U_{\mathrm{RM2}}$, i_{RM1},i_{RM2} are the real voltages and currents of redundancy modules in the upper and bottom arms, respectively; K_{p2} is the proportional coefficient.

The block diagram of the redundancy module controller is shown in Fig. 3.

C. Voltage Stability Controller

The purpose of the voltage stability controller is to balance the three-phase voltages and reduce the circulation current between phases. The detailed block diagram of the voltage stability controller is shown in Fig. 4, which includes a voltage loop and a current loop. The PI regulators are used for both loops. Here, U_C is half of the sum capacitor voltages of each phase, which could be calculated by (13), where $U_{\mathrm{PV}k}$ is the capacitor voltage in kth PM; $U_{C\mathrm{ref}}$ is the reference value of U_C and generally equals to U_{DCref}; i_{cir} is the circulation current between phases, and it can be calculated by (14); i_p and i_n are the currents of upper and bottom bridge arms of phase A, respectively, as shown in Fig. 1

$$U_C = \frac{1}{2}\left[\left(\sum_{k=1}^{n} U_{\mathrm{PV}k}\right) + U_{\mathrm{RM1}} + U_{\mathrm{RM2}}\right] \tag{13}$$

$$i_{\mathrm{cir}} = \frac{i_p + i_n}{2}. \tag{14}$$

D. Grid-Connected Controller

A voltage-loop regulator is used to keep the common dc-bus voltage constant [37]. The output of the voltage-loop regulator is used as the command current in *d*-axis, while the *q*-axis command current is assigned directly by the reactive power requirement of the ac utility. The block diagram of the proposed grid-connected controller is shown in Fig. 5. First, U_{DC} is compared to its reference voltage U_{DCref}. The difference goes through a PI regulator to follow the active current reference $i_{d\mathrm{ref}}$. On the other hand, the reactive current reference $i_{q\mathrm{ref}}$ is decided by the PV system requirement for reactive power compensation. For simplicity, $i_{q\mathrm{ref}}$ is set to zero, which means no reactive power will be provided by the PV system. Finally, another two PI regulators are used to regulate the real active current i_d and reactive current i_q output from the MMC to follow $i_{d\mathrm{ref}}$ and $i_{q\mathrm{ref}}$, respectively.

The MPPT controller, redundancy module controller, voltage stability controller, and grid-connected controller are implemented by using the modulation of carrier phase shift [38]. The control reference signals for the PMs are

$$U_{\mathrm{PM}} = U_{\mathrm{ref1}} + U_{\mathrm{ref3}} + \frac{U_{\mathrm{DC}}}{2N} - \frac{U_{\mathrm{ref4}}}{N} \text{ (Upper arm)} \tag{15}$$

$$U_{\mathrm{PM}} = U_{\mathrm{ref1}} + U_{\mathrm{ref3}} + \frac{U_{\mathrm{DC}}}{2N} + \frac{U_{\mathrm{ref4}}}{N} \text{ (Bottom arm)}. \tag{16}$$

The control reference signals for the RMs are

$$U_{\mathrm{RM}} = U_{\mathrm{ref2\_up}} + U_{\mathrm{ref3}} + \frac{U_{\mathrm{DC}}}{2N} - \frac{U_{\mathrm{ref4}}}{N} \text{ (Upper arm)} \tag{17}$$

$$U_{\mathrm{RM}} = U_{\mathrm{ref2\_down}} + U_{\mathrm{ref3}} + \frac{U_{\mathrm{DC}}}{2N} + \frac{U_{\mathrm{ref4}}}{N} \text{ (Bottom arm)}. \tag{18}$$

IV. Simulation Analyses

In the simulation model, the cascaded number of N = 2 is adopted to verify the performance of the proposed topology and

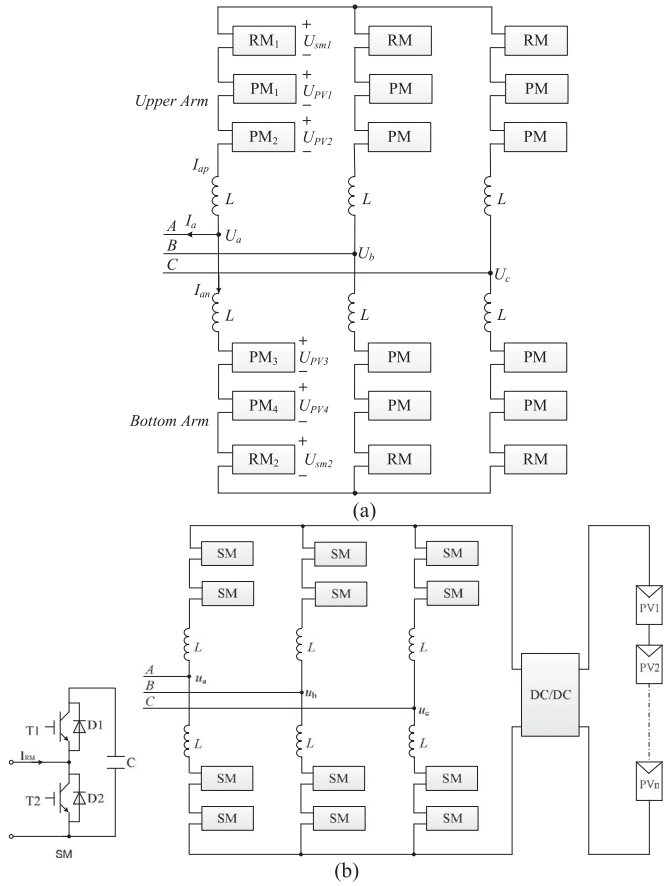

Fig. 6. Topology for simulation. (a) Proposed topology. (b) Traditional topology.

TABLE II
PARAMETERS OF THE MAIN CIRCUIT

Parameters	Value
AC terminal voltage	380 V (phase to phase)
Capacitor of PMs and RMs	2000 μF/each
Inductor	10 mH/each
Switching frequency	20 kHz
U_{DCref}	600 V

control methods, especially the ability of adjusting the capacitor voltages of PMs under partial shading conditions, and the possibility to realize the independent MPPT for each PV module. Each bridge arm is composed with two PM modules, one RM module, and one inductor, as shown in Fig. 6(a), and the traditional topology mentioned in [32] is also setup for comparison, which is shown in Fig. 6(b). Both topologies will be simulated under the same conditions. The parameters of main circuit are given in Table II, while the parameters of the controller are given in Table III. The parameters of PV module are given in Table IV, the *I–V* curves of PV module under different irradiance are shown in Fig. 7.

TABLE III
PARAMETERS OF CONTROLLER

Parameters	Value
K_{P1}	5
K_{P2}	3
K_{P3}	1
K_{I3}	500
K_{P4}	5
K_{I4}	100
K_{P5}	1
K_{I5}	200
K_{P6}	0.6
K_{I6}	100

TABLE IV
PARAMETERS OF PV MODULES

Irradiance /(W/m^2)	Open voltage V_{oc}(V)	Short current I_s(A)	MPP voltage V_{MPP}(V)	Maximum power P_{max}(W)	$R_{\mathrm{sh}}(\Omega)$	$R_s(\Omega)$
200	334	0.8	280	192.3	260	0.35
400	346	1.6	294	420.6		
800	357	3.2	299	880.8		
1000	360	4.1	305	1109.0		

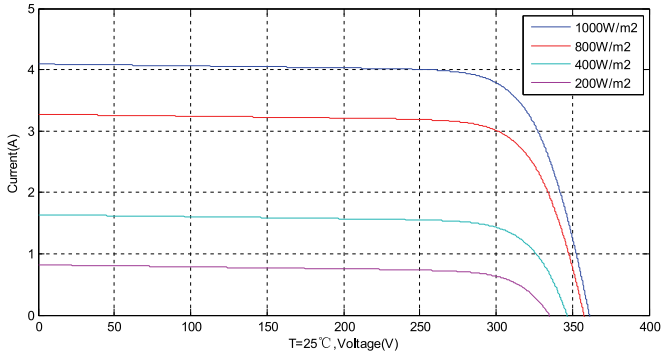

Fig. 7. *I–V* curves of PV module under different irradiance.

TABLE V
DETAIL SHADING CONDITIONS IN SIMULATION

Module	Time(s)	
	0 to 0.5	0.5 to 1.0
PM1 (W/m^2)	1000	200
PM2 (W/m^2)	1000	800
PM3 (W/m^2)	1000	400
PM4 (W/m^2)	1000	1000

A. Case 1. Partial shading With the Proposed Topology and Control Method

In this case, the irradiance of all PMs is set to 1000 W/m^2 initially. After 0.5 s, the irradiance is changed to 200, 800, 400, and 1000 W/m^2, respectively. The detail shading conditions are given in Table V.

The simulation results are shown in Fig. 8. Fig. 8(a) shows the capacitor voltages of two PMs in upper arm of phase A. Both of the voltages are about 300 V initially, and then change to 278 and 300 V with a ripple of about 6 V, respectively. Because the output power of the PV module is closely related to its output voltage, the ripple of capacitor voltage of PM will decrease the output power of PV module. The capacitance value of PM needs to be increased to reduce this voltage ripple. According to the *P–U* characteristics of the PV module, it is known that within a short range near the MPP, the change of output voltage has a little effect on the output power of the PV module. Therefore, this paper selects the capacitance to be 2000 μF, and with this capacitance value, the voltage ripple is reduced to be less than 3%, the power loss is less than 1%.

Fig. 8(b) shows the capacitor voltages of two PMs in the bottom arm. The voltages change from 300 to 292 V and 302 V, respectively, which is caused by the MPPT controller. From Table IV, it is known that all PV modules still operate at their MPP even under partial shading. Fig. 8(c) shows the capacitor voltages of two RMs. The value is near 0 V initially, and that means the redundancy modules do not work under nonshading conditions. After 0.5 s, the capacitor voltages of RM1 and RM2 increase to 14, 5 V, respectively. It means that the redundancy module can compensate the voltage loss which is caused by partial shading. Fig. 8(d) shows the output power waveform of phase A. Its value is about 4400 W before 0.5 s and 2585 W after 0.5 s. This value is very close to the theoretical value, 2602 W, which can be calculated from Table IV.

Fig. 8(e) shows the output waveforms of the PV module in PM1. The output current is 3.65 A initially, and then drops to 0.56 A immediately at 0.5 s for the irradiance changing to 200 W/m^2. With the adjustment of MPPT controller, the current come back to 0.65 A at 0.52 s. The output power is dropped from 1106 to 170 W at 0.5 s and come back to 192 W at 0.52 s. These results are very close to the theoretical value which justifies the effectiveness of the MPPT controller.

Note that the voltage reference of RMs is 0 V before 0.5 s, but the capacitor voltages of RMs cannot be a negative value. Hence, during the discharge process, the capacitor voltages of the RMs could only be reduced to 0 V, and during the charging process, the capacitor voltages start to rise. In view of the overall process, the average value of the capacitor voltage has an offset from zero. The offset is not big, and its influence can be ignored. Furthermore, when the RMs need to contribute a big voltage compensation, the offset will disappear automatically.

B. Case 2. Some PM is Burnt Out Suddenly

In this case, the irradiance of all PMs of phase A is set to 1000 W/m^2 initially. After 0.5 s, the PV module in PM1 is burnt out, and the output current of this PV module drops to zero immediately. The simulation results are shown in Fig. 9. Fig. 9(a) and (b) are the capacitor voltages of PMs in upper arm and bottom arm, respectively. The voltage of capacitor in each PM is about 300 V before 0.5 s, which means that all PV modules work at their MPP. After 0.5 s, the capacitor voltage of PM1 is slightly decreased to 294 V, and then go back up to

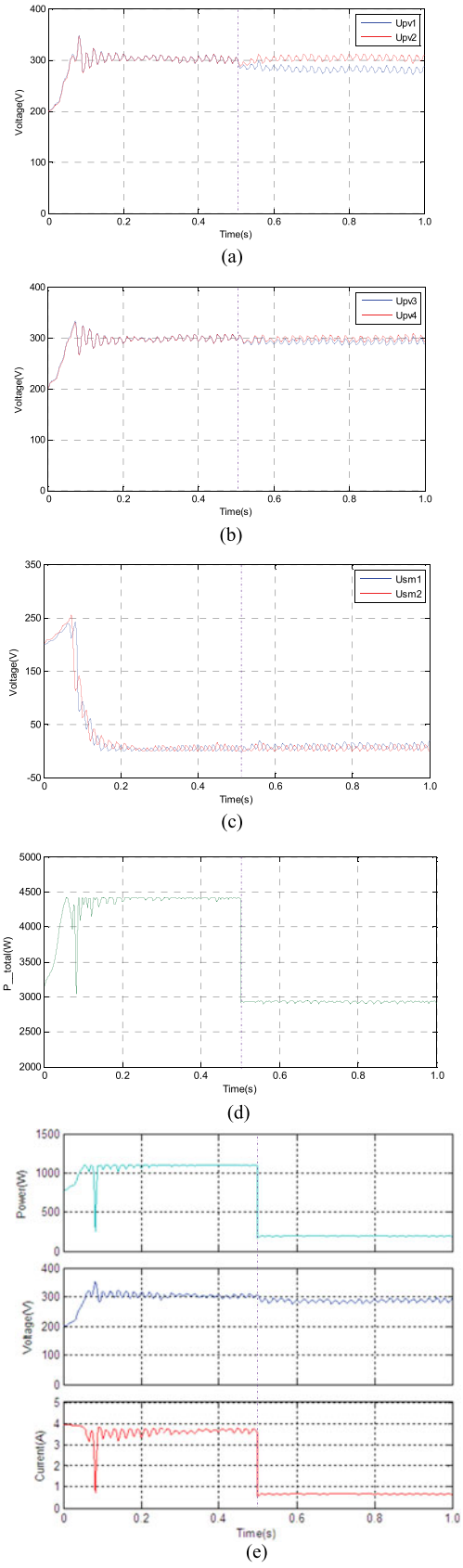

Fig. 8. Voltage and power waveforms under partial shading. (a) Capacitor voltages of PM1 and PM2. (b) Capacitor voltages of PM3 and PM4. (c)Capacitor voltages of RM1 and RM2. (d) Output power waveform. (e) Output waveforms of PV1 module in PM.

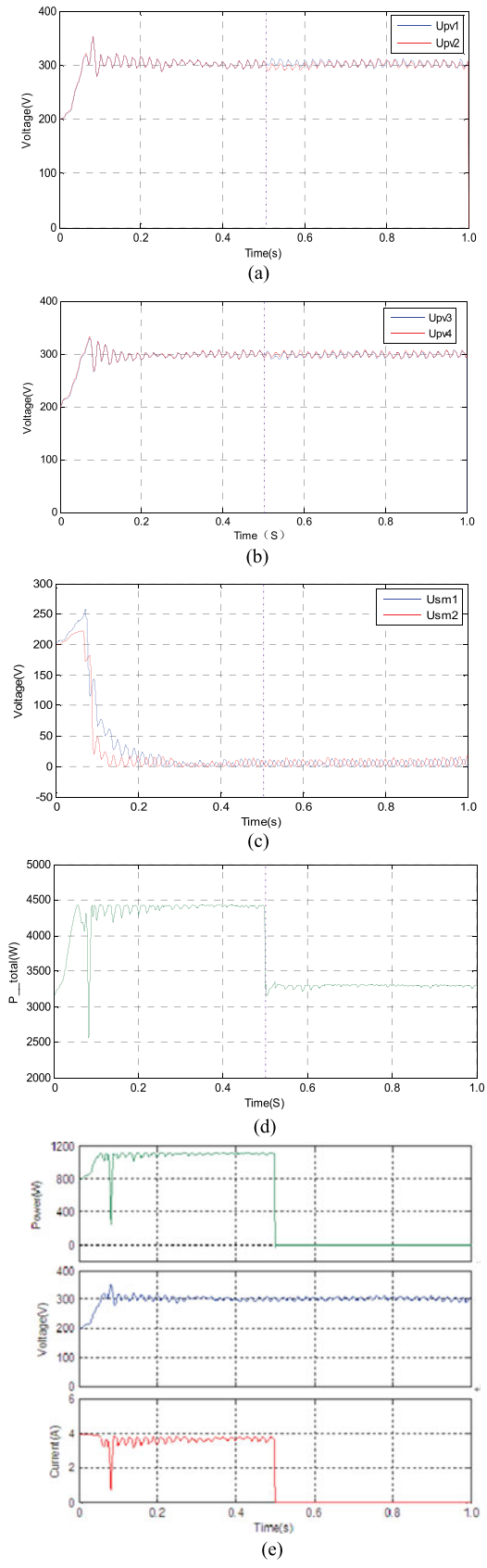

Fig. 9. Voltage and power waveforms when PM1 is burnt out. (a) Capacitor voltages of PM1 and PM2. (b) Capacitor voltages of PM3 and PM4. (c) Capacitor voltages of RM1 and RM2. (d) Output power waveform. (e) Output waveforms of PV module in PM1.

300 V at 0.6 s. However, the other PMs still work at their MPP, keeping the capacitor voltages at 300 V.

Fig. 9(c) shows the capacitor voltages of RM modules. The capacitor voltages of RM1 and RM2 are near 0 V all the time. It is because that when any PV module is burnt out, the corresponding PM works as a RM. So theoretically speaking, the voltage loss can be compensated no matter how many PMs are burnt out.

Fig. 9(d) shows the output power. The value is about 4400 W before 0.5 s and 3300 W after 0.5 s. Fig. 9(e) shows the output waveforms of the PV module in PM1. The current is 3.6 A before 0.5 s, and then drops to zero immediately for the reason that the PV module is burnt out, and the output power is dropped from 1106 W to 0 immediately too. These simulation results consist with the theoretical analysis well.

C. Case 3. Partial Shading With the Traditional Topology and Control Method

In this case, the PV modules are connected in series. They are first boosted by a dc–dc chopper, and then connected to the grid by MMC circuit. The P&O method is adopted for the MPPT control. The irradiance of all PV modules is set to be the same as that in case 1. The *P–U* characteristic curve, output power waveform, and voltages of PV modules are shown in Fig. 10. As can be seen from Fig. 10, the output power is about 4400 W initially, and then changes to 921 W after 0.5 s. Compared to case 1, the output power is almost the same as that of case 1 before 0.5 s, but is much lower after 0.5 s. The reason is that not all PV modules work at their MPP under partial shading in the case of using the traditional topology and control method.

Note that the MPPT is plunged in local MPP D, as shown in Fig. 10(a). It is because that the terminal voltage of the series PV branch is about 1200 V initially before partial shading occurs. The P&O MPPT method will only search in the region IV and ultimately converge to point D. The terminal voltage of the series PV branch ultimately increases to 1288 V, as shown in Fig. 10(c). Even the global MPP is found (point B), for example, take the global MPPT method in [14] and [15], the output power is about 1893 W, which is still far less than that of case 1.

D. Case 4. Some PV Module is Burnt Out With the Traditional Topology and Control Method

Suppose all PV modules work at MPPs, the terminal voltage of each PV module is V_{mpp}, the number of PV modules is k, then the terminal voltage of the series PV branch is kV_{mpp}. When some PV module is burnt out, kV_{mpp} will be distributed to the rest $(k-1)$ PV modules. Therefore, the terminal voltages of the rest PV modules will be higher than their MPP voltages, which will decrease the output power of the PV system.

The simulation results are shown in Fig. 11. The output power is changed from 4400 W (before 0.5 s) to 0 W (between 0.5 and 0.58 s) and then to 3300 W (after 0.58 s). Compared with the proposed topology, a gap exists in the power waveform, which is due to the intrinsic characteristics of the P&O MPPT method. The reason is that when some PV module is burnt out, the input voltage of the dc–dc chopper will be imposed on the new series

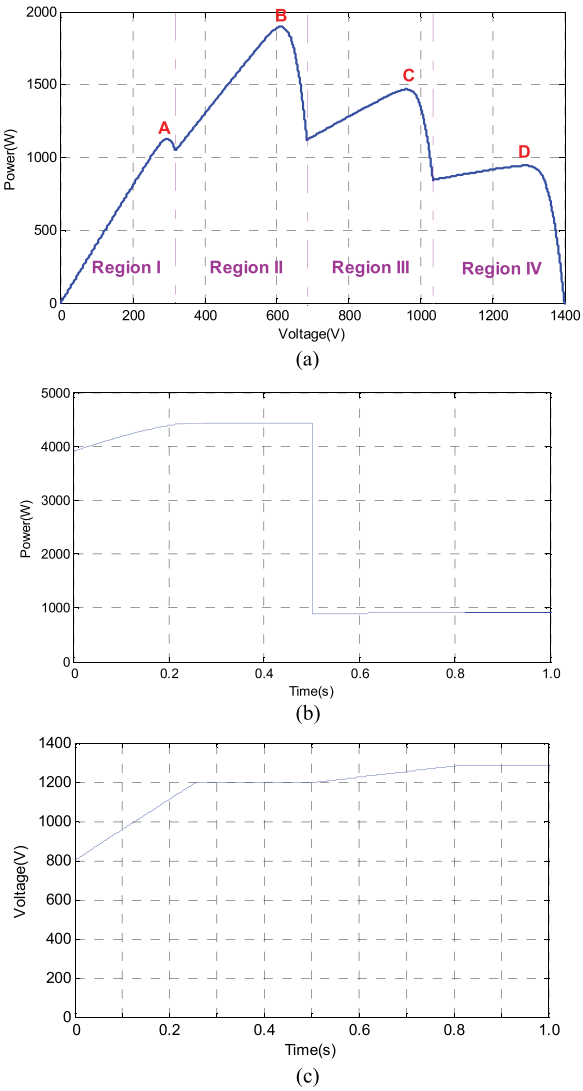

Fig. 10. Power waveforms with the traditional topology and control method. (a) *P–U* characteristic curve under partial shading. (b) Output power. (c) Output voltage of PV array.

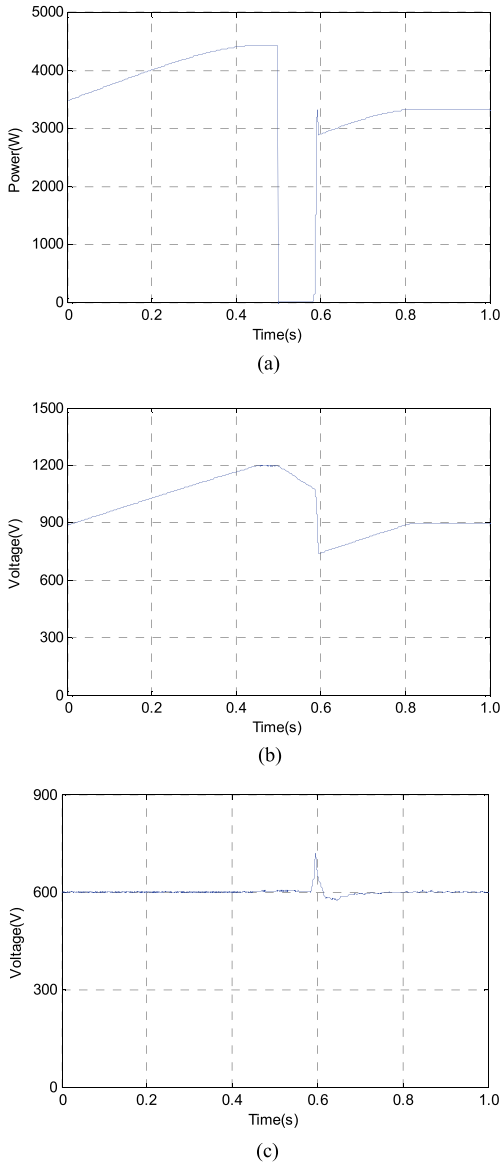

Fig. 11. Power and voltage waveforms with the traditional topology when some PV module is burnt out. (a) Output power. (b) Input voltage of the dc–dc chopper. (c) DC voltage of MMC.

PV branch with $k-1$ modules, which exceeds the open-circuit voltage of the new series PV branch, so the output power is zero. At 0.58 s, the input voltage of the dc–dc chopper declines to less than the open-circuit voltage of the new series PV branch, the output power is gradually increased to the new MPP, which is 3300 W. If take some intelligent global MPPT method, the gap maybe narrow, but will not disappear.

E. Case 5. Reconfigure Structure Under Partial Shading

In this case, the structure of PV array under partial shading is reconfigured, as proposed in [27].The initial structure is shown in Fig. 12(a), while the final structure is shown in Fig. 12(b). The irradiance of all PV modules is set to be the same as that of case 1. At 0.5 s, the structure is changed from initial structure to final structure by some switches.

The *P–U* characteristic curve, output power waveform, and voltage waveforms are given in Fig. 13. From Fig. 13(a), it can

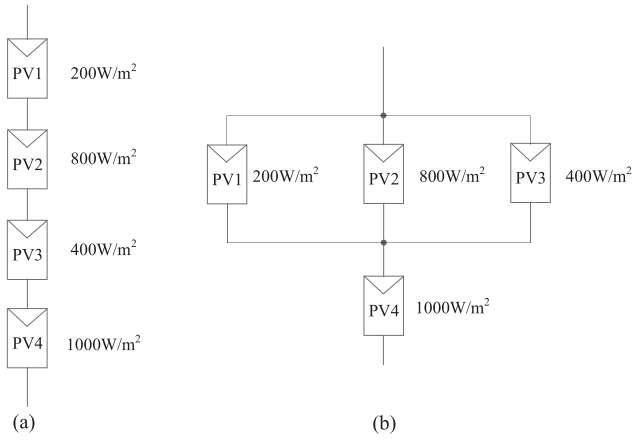

Fig. 12. Structure of PV array. (a) Initial structure. (b) Final structure.

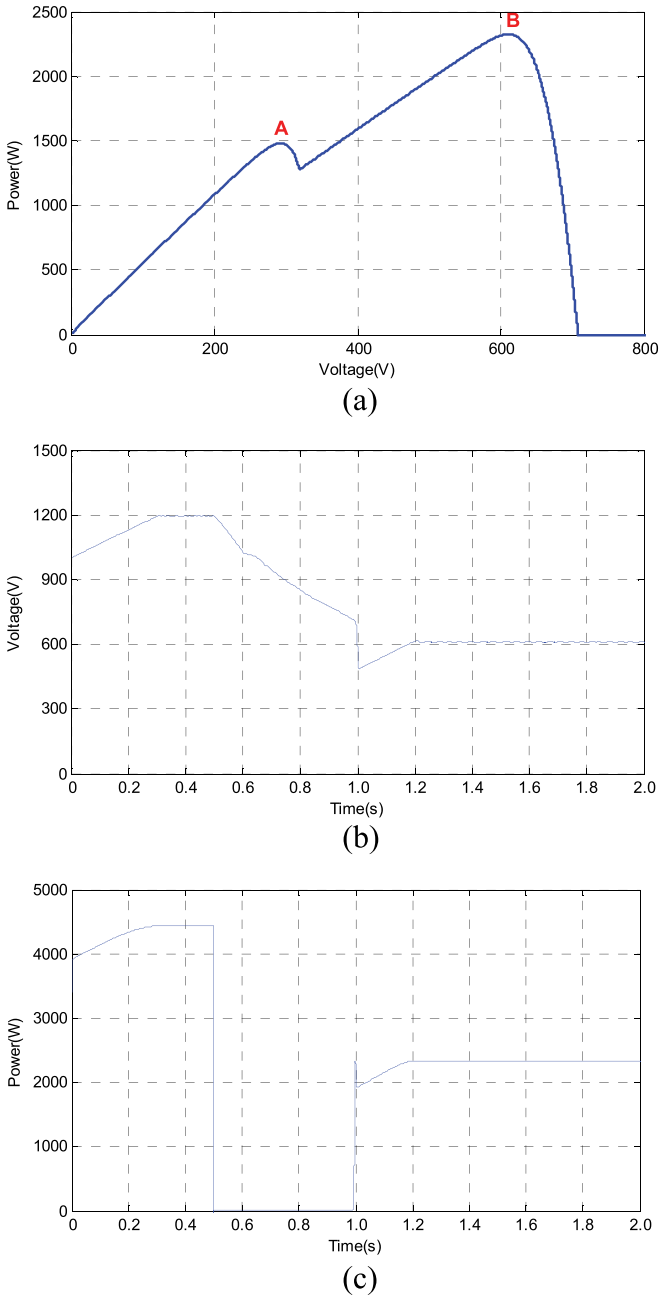

Fig. 13. Power and voltage waveforms with reconfigure structure under partial shading. (a) *P–U* characteristic curve under partial shading. (b) Output power. (c) Output voltage of PV array.

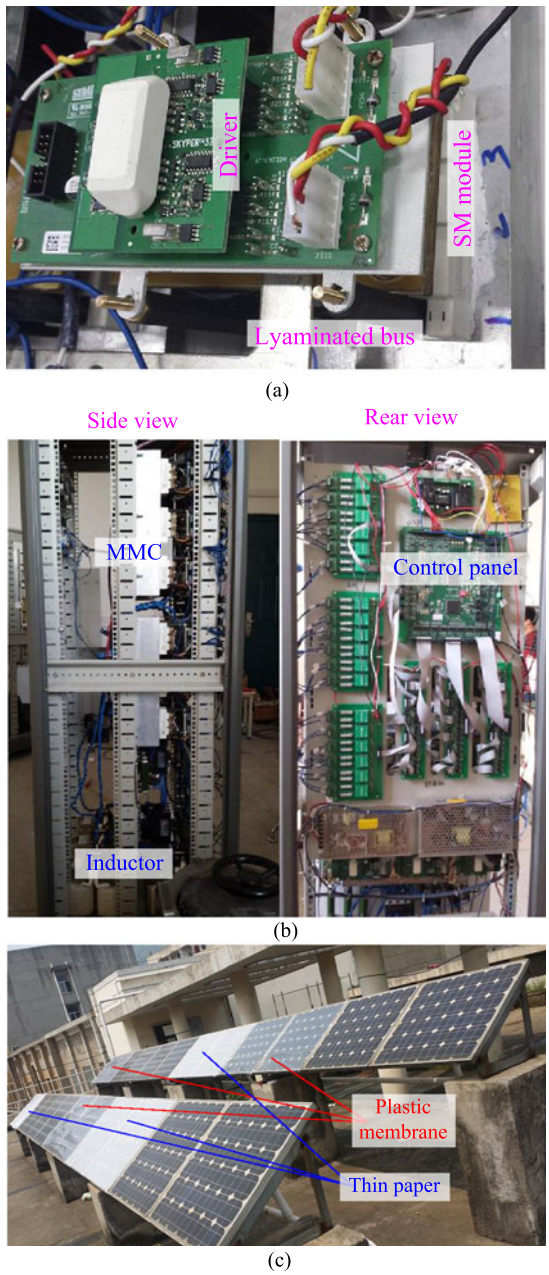

Fig. 14. Experimental platform. (a) SM module. (b) Main circuit. (c) PV array.

be seen that there are only two maximum points in the *P–U* characteristic curve, which is half of those in Fig. 10(a). So, the global MPPT will be easier to realize. The output power is about 4400 W initially, and suddenly drops to 0 W, which is because that the structure of PV array is reconfigured, and the terminal voltage of PV array exceeds its open-circuit voltage, as shown in Fig. 13(b) clearly. The terminal voltage of PV array is 1195 V before 0.5 s and then decreases to 610 V gradually. That means the MPPT method converges to point B, and the output power of PV array reaches to 2323 W, which is more than that of traditional topology, but still less than that of the proposed topology.

V. Experiment Results

A 3-kW PV experimental platform is set up, which consists of 24 PV modules, as shown in Fig. 14. Each PV module has a maximum power of 121 W and the MPP voltage is 28.5 V in the standard circumstance (25 °C, 1000 W/m^2), the *I–U* and *P–U* curves are shown in Fig. 15. The other parameters of experimental platform are given in Table VI.

A four level three-phase MMC is used as the grid-connected converter, as shown in Fig. 16. Each arm has three submodules. One submodule works as RM, two other submodules work as PMs. Accordingly, 12 submodules are needed for this experiment. Every two PV modules are connected in series as a group

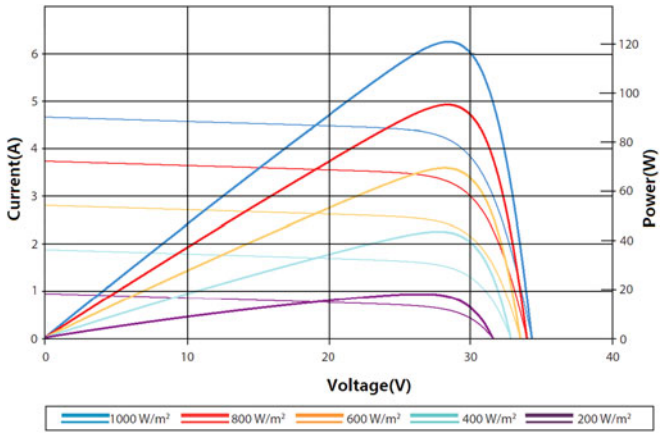

Fig. 15. Current–voltage and power–voltage curves.

TABLE VI
PARAMETERS OF EXPERIMENTAL PLATFORM

Parameters	Value
Grid voltage (phase to phase)	380 V
Frequency	50 Hz
Power	3 kW
PV groups	12
Number of PV modules per group	2
Transform ratio	5:1

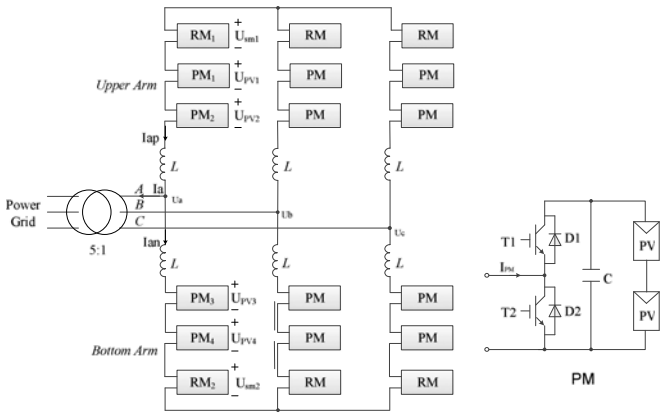

Fig. 16. Topology of PV experimental platform.

to connect to the capacitor of each submodule. That is to say, when the number of PV modules is much bigger than that of submodules of MMC, the PV modules can first be grouped and then connected to MMC. It needs to be noted that, in this condition, the bypass diodes must be reserved to avoid the internal hotspot in the PV group. A boost transformer with a ratio of 5:1 is used to connect the PV system to the grid.

A. Partial Shading

To imitate the partial shading, the first PM is covered by a transparent plastic membrane, the last PM is covered by a piece of thin paper for each phase, the detailed shading conditions are

TABLE VII
DETAIL SHADING CONDITIONS IN EXPERIMENT

Parameters	Value
Temperature	30 °C
Irradiance	910 W/m^2
Shading factor of thin paper	0.29
Shading factor of plastic membrane	0.78

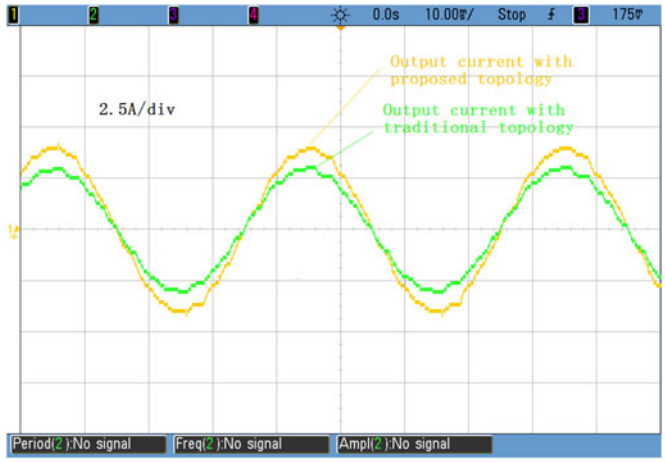

Fig. 17. Output current waveforms.

described in Table VII. The control parameter U_{Dcref} is set to 120 V.

The experimental results are shown in Fig. 17. In the case of the traditional topology, the output current of phase A is 2.31 A, the total output power is about 1.53 kW. However, as a comparison, in the case of the proposed topology, the output current of phase A is increased by 19% to 2.75 A, and the total output power is also increased by 19% to 1.82 kW.

Fig. 18 shows the capacitor voltages of PMs and RMs in phase A. It needs to be noted that the ratio of the voltage sensor is 10:1. The capacitor voltages of PM1, PM2, PM3, PM4 are 54.8, 57.3, 57.5, 50.7 V, respectively. The capacitor voltages of RM1, RM2 are 8.4, 12.3 V, respectively. All of the capacitor voltages are much lower than the dc-bus voltage, which indicates that the novel topology has lower voltage stress on switching device. Compared with the traditional topology, the THD is slightly increased from 4.1% to 4.7%, which still meets the national standard requirements.

B. Some PM is Burnt Out Suddenly

In order to imitate the condition of burning out some PM, the PV module in PM1 is connected with a switch in parallel. When switching on this switch, the PV module is bypassed and can be regarded as burning out. The experimental results are shown in Fig. 19. From Fig. 19(b), it can be seen that the capacitor voltage waveform has a fluctuation at first, and finally reach the stable state at 57 V. It is because that when PM1 is burnt out, the output power is reduced to zero, and the MPPT controller controls the capacitor voltage to be the same as that of before burning out.

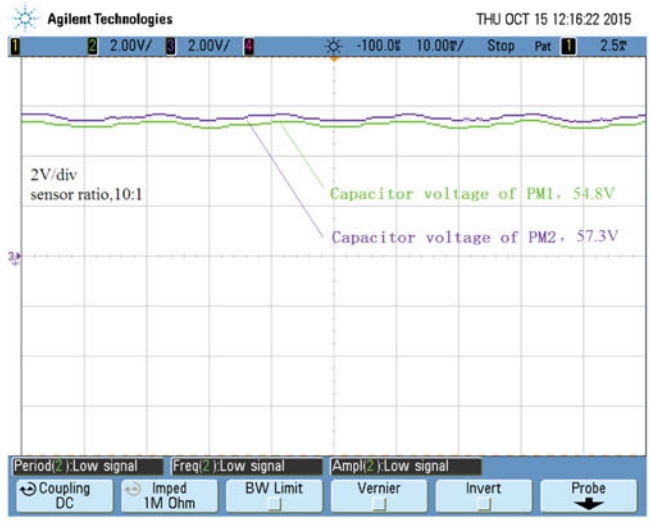

(a)

(b)

(c)

Fig. 18. Capacitor voltages of PMs and RMs. (a) Voltages of PM1 and PM2. (b)Voltages of PM3 and PM4. (c) Voltages of RM1 and RM2.

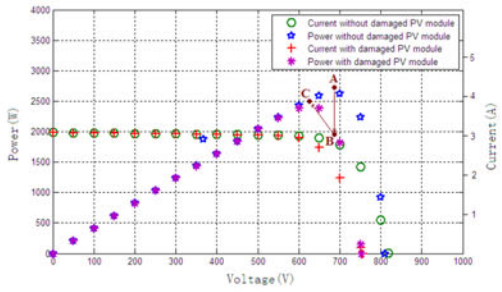

(a)

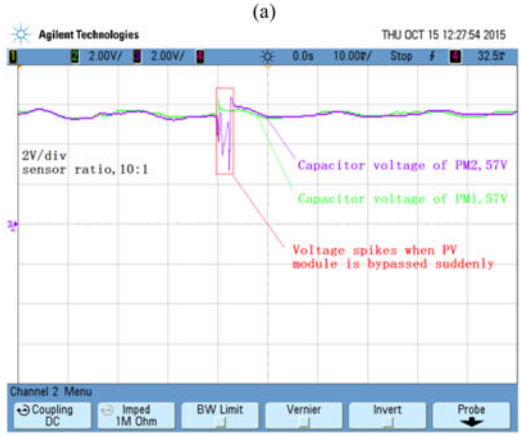

(b)

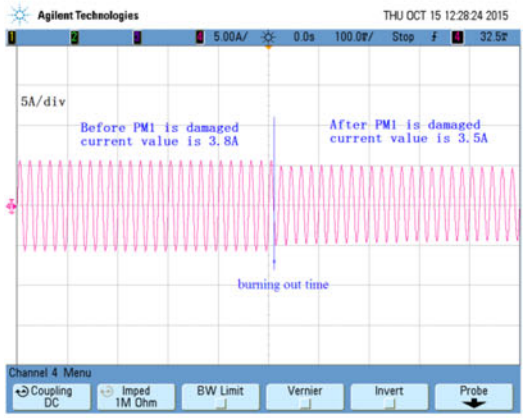

(c)

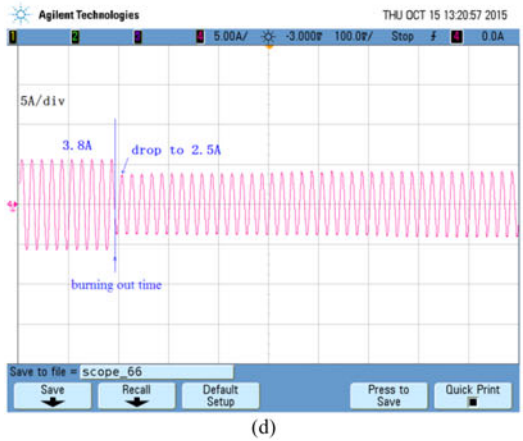

(d)

Fig. 19. Experiment results when some PM is burnt out. (a) *I–U* and *P–U* curves. (b) Voltage of PMs in upper arm when using the proposed topology. (c) Output current when using the proposed topology. (d) Output current when using the traditional topology.

Fig. 19(c) shows the output current waveform when employing the proposed topology, the value is changed from 3.8 to 3.5 A. The output power is changed from 2.50 to 2.31 kW.

When using the traditional topology, the first two PV modules are connected with a switch in parallel. The output current waveform is shown in Fig. 19(d). From Fig. 19(d), it can be seen that the current value is changed from 3.8 to 2.5 A when switching on the switch, and then increased gradually. After the scope is refreshed three times, the output current can reach the stable state at 3.5 A. This is because that when the first two PV modules are bypassed by the switch, the dc-bus voltage is exposed on the rest PV modules, all PV modules cannot work at their MPPs, but with the adjustment of the MPPT controller, the dc-bus voltage returns to the MPP voltage again. The *I–U* and *P–U* curves of the PV array are shown in Fig. 19(a). Before burning out time, the PV system works at point A, and then it changes to point B immediately when the first two PV modules are bypassed; finally, the work point goes back to point C under the function of the MPPT controller.

VI. Conclusion

In this paper, a novel topology for the PV array is proposed, where a PV module is connected to the capacitor of each submodule of MMC in parallel. It aims to improve the output power under partial shading by regulating the voltage of capacitor in each PM to the MPP voltage of PV module. A RM is designed and connected to each bridge arm of the MMC to compensate the voltage loss caused by the irradiance variation. The proposed PV topology has lower voltage stress on switching device and higher efficiency.

The control strategy has four parts: 1) the maximum power tracking controller, 2) the redundancy module controller, 3) the voltage stability controller, and 4) the grid-connected controller. Experimental verifications were performed by building a 3-kW PV system experimental platform. Simulation and experimental results show that the proposed topology has the same efficiency as that of the traditional topology under nonshading, but achieves higher efficiency under partial shading, and compared with the reconfiguration structure, the proposed topology not only eliminates the complexity of the reconfiguration structure, but also achieves the ability of higher output power under partial shading.

References

[1] I. R. Balasubramanian, S. I. Ganesan, and N. Chilakapati, "Impact of partial shading on the output power of PV systems under partial shading conditions," *IET Power Electron.*, vol. 7, no. 3, pp. 657–666, 2014.

[2] K. Chen *et al.*, "An improved MPPT controller for photovoltaic system under partial shading condition," *IEEE Trans. Sustainable Energy*, vol. 5, no. 3, pp. 978–985, Jun. 2014.

[3] M. Z. S. El-Dein, M. Kazerani, and M. M. A. Salama, "Optimal photovoltaic array reconfiguration to reduce partial shading losses," *IEEE Trans. Sustainable Energy*, vol. 4, no. 1, pp. 145–153, Jan. 2013.

[4] A. Qahouq and J. A. Yuncong Jiang, "Distributed photovoltaic solar system architecture with single-power inductor single-power converter and single-sensor single maximum power point tracking controller," *IET Power Electron*., vol. 7, no. 10, pp. 2600–2609, 2014.

[5] A Alisson Alencar Freitas *et al.*, "High-voltage gain dc–dc boost converter with coupled inductors for photovoltaic systems," *IET Power Electron.*, vol. 8, no. 10, pp. 1885–1892, 2015.

[6] G. Acciari, D. Graci, and A. L. Scala, "Higher PV module efficiency by a novel CBS bypass," *IEEE Trans. Power Electron.*, vol. 26, no. 5, pp. 1333–1336, May 2011.

[7] R. P. Vengatesh and S. E. Rajan, "Investigation of the effects of homogeneous and heterogeneous solar irradiations on multicrystal PV module under various configurations," *IET Renew. Power Gener.*, vol. 9, no. 3, pp. 245–254, 2015.

[8] A. Bidram, A. Davoudi, and R. S. Balog, "Control and circuit techniques to mitigate partial shading effects in photovoltaic arrays," *IEEE J. Photovoltics*, vol. 2, no. 4, pp. 532–546, Oct. 2012.

[9] J. D. Bastidas-Rodriguez *et al.*, "Maximum power point tracking architectures for photovoltaic systems in mismatching conditions," *IET Power Electron*., vol. 7, no. 6, pp. 1396–1413, 2014.

[10] S. Lyden and Md. E. Haque, "A simulated annealing global maximum power point tracking approach for PV modules under partial shading conditions," *IEEE Trans. Power Electron.*, vol. 31, no. 6, pp. 4171–4181, Jun. 2016.

[11] P. Sharma and V. Agarwal, "Exact maximum power point tracking of grid-connected partially shaded PV source using current compensation concept," *IEEE Trans. Power Electron.*, vol. 29, no. 9, pp. 4684–4692, Sep. 2014.

[12] Md. A. Ghasemi, H. M. Forushani, and M. Parniani, "Partial shading detection and smooth maximum power point tracking of PV arrays under PSC," *IEEE Trans. Power Electron.*, vol. 31, no. 9, pp. 6281–6292, Sep. 2016.

[13] R. Alik, A. Jusoh, and N. A. Shukri, "An improved perturb and observe checking algorithm MPPT for photovoltaic system under partial shading condition," in *Proc. IEEE Conf. Energy Convers.,* Johor Bahru, Malaysia, Oct. 2015, pp. 398–402.

[14] M. Seyedmahmoudian *et al.*, "Simulation and hardware implementation of new maximum power point tracking technique for partially shaded PV system using hybrid DEPSO method," *IEEE Trans Sustainable Energy*, vol. 6, no. 3, pp. 850–862, Jul. 2015.

[15] K. Sundareswaran *et al.*, "Enhanced energy output from a PV system under partial shaded conditions through artificial bee colony," *IEEE Trans Sustainable Energy*, vol. 6, no. 1, pp. 198–209, Jan. 2015.

[16] H. Sekhar Sahu, S. Kumar Nayak, and S. Mishra, "Maximizing the power generation of a partially shaded PV array," *IEEE J. Emerging Sel. Topics Power Electron.*, vol. 4, no. 2, pp. 626–637, Jun. 2016.

[17] A. Ahmed *et al.*, "A switched PV approach for extracted maximum power enhancement of PV arrays during partial shading," *IEEE Trans. Sustainable Energy*, vol. 6, no. 3, pp. 767–772, Jul. 2015.

[18] J. Ahmad, A. Ciocia, and F. Spertino, "A maximum power point tracker of photo voltaic arrays for partial shading conditions," in *Proc. Int. Conf. Ind. Eng. Oper. Manage.*, Dubai, UAE, Mar. 2015, pp. 1–5.

[19] S. Zengin, F. Deveci, and M. Boztepe, "Volt-second-based control method for discontinuous conduction mode flyback micro-inverters to improve total harmonic distortion," *IET Power Electron.*, vol. 6, no. 8, pp. 1600–1607, 2013.

[20] I. Abdalla, J. Corda, and L. Zhang, "Multilevel DC-link inverter and control algorithm to overcome the PV partial shading," *IEEE Trans. Power Electron.*, vol. 28, no. 1, pp. 14–18, Jan. 2013.

[21] S. Essakiappan *et al.*, "Multilevel medium-frequency link inverter for utility scale photovoltaic integration," *IEEE Trans. Power Electron.*, vol. 30, no. 7, pp. 3674–3684, Jul. 2015.

[22] H. Ghoddami and A. Yazdani, "A single-stage three-phase photovoltaic system with enhanced MPP tracking capability and increased power rating," *IEEE Trans. Power Del.*, vol. 26, no. 2, pp. 1017–1029, Apr. 2011.

[23] M. Z. S. El-Dein, M. Kazerani, and M. M.A. Salama, "Optimal photovoltaic array reconfiguration to reduce partial shading losses," *IEEE Trans. Sustainable Energy*, vol. 4, no. 1, pp. 145–153, Jan. 2013.

[24] B. I. Rani, G. S. Ilango, and C. Nagamani, "Enhanced power generation from PV array under partial shading conditions by shade dispersion using Su Do Ku configuration," *IEEE Trans. Sustainable Energy*, vol. 4, no. 3, pp. 594–601, Jul. 2013.

[25] A. L. Lentine, G. N. Nielson, and M. Okandan, "Optimal cell connections for improved shading, reliability, and spectral performance of microsystem enabled photovoltaic (MEPV) modules," in *Proc. IEEE Photovoltics Spec. Conf.*, 2010, pp. 3048–3054.

[26] L. Al Nufaie and A. A. Hafez, "Fuzzy optimisation of a photovoltaic installation," in *Proc. IET Int. Conf. Power Electron.*, 2014, pp. 1–6.

[27] L. F. Lavado Villa *et al.*, "Maximizing the power output of partially shaded photovoltaic plants through optimization of the interconnections among its modules," *IEEE J. Photovoltics*, vol. 2, no. 2, pp. 154–163, Apr. 2012.

[28] R. P. Vengatesh and S. Edward Rajan, "Investigation of the effects of homogeneous and heterogeneous solar irradiations on multicrystal PV module under various configurations," *IET Renew. Power Gener.*, vol. 9, no. 3, pp. 245–254, 2015.
[29] L. F. L. Villa, B. Raison, and J.-C. Crebier, "Toward the design of control algorithms for a photovoltaic equalizer: Detecting shadows through direct current sampling," *IEEE J. Emerging Sel. Topics Power Electron.*, vol. 2, no. 4, pp. 893–906, Dec. 2014.
[30] A. Alexander and M. Thathan, "Modelling and analysis of modular multilevel converter for solar photovoltaic applications to improve power quality," *IET Renew. Power Gener.*, vol. 9, no. 1, pp. 78–88, 2015.
[31] G. Ramya and R. Ramaprabha, "Design methodology of P-Res controllers with harmonic compensation technique for modular multilevel converter fed from partially shaded PV array," in *Proc. Int. Conf. Power Electron. Drive Syst.*, Sydney, Australia, Jun. 2015, pp. 330–335.
[32] G. Ramya and R. Ramaprabha, "Switching loss and THD analysis of modular multilevel converter with different switching frequency," in *Proc. Int. Conf. Power Electron. Drive Syst.*, Sydney, Australia, Jun. 2015, pp. 336–340.
[33] S. Rivera *et al.*, "Modular multilevel converter for large-scale multistring photovoltaic energy conversion system," in *Proc. IEEE Conf. Energy Convers. Congr. Expo.*, Denver, CO, USA, Sep. 2013, pp. 1941–1946.
[34] J. Echeverría, S. Kouro, and M. Pérez, "Multi-modular cascaded DC-DC converter for HVDC grid connection of large-scale photovoltaic power systems," in *Proc. IEEE Conf. Ind. Electron. Soc.*, Vienna, Austria, Nov. 2013, pp. 6999–7005.
[35] J. Mei *et al.*, "Modular multilevel inverter with new modulation method and its application to photovoltaic grid-connected generator," *IEEE Trans. Power Electron.*, vol. 28, no. 11, pp. 5063–5073, Nov. 2013.
[36] S. Rajasekar *et al.*, "Solar photovoltaic power conversion using modular multilevel converter," in *Proc. Students Conf. Eng. Syst.*, 2012, pp. 1–6.
[37] S. Du, J. Liu, and T. Liu, "Modulation and closed-loop-based DC capacitor voltage control for MMC with fundamental switching frequency," *IEEE Trans. Power Electron.*, vol. 30, no. 1, pp. 327–338, Jan. 2015.
[38] B. Li *et al.*, "Analysis of the phase-shifted carrier modulation for modular multilevel converters," *IEEE Trans. Power Electron.*, vol. 30, no. 1, pp. 297–310, Jan. 2015.

Fei Rong was born in Hubei, China, in 1978. He received the B.S. and M.S. degrees from Central South University, Changsha, China, in 2000 and 2003, respectively, and the Ph.D. degree from Hunan University, Changsha, in 2008.

He was a Lecturer from 2008 to 2010, and since 2011, he has been an Associate Professor of electrical engineering with the College of Electrical and Information Engineering, Hunan University. His research interests include distributed power generation, reactive power compensation, and active power filters.

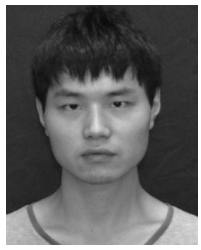

Xichang Gong was born in Hunan, China, in 1992. He received the B.S. degree from Hunan University of Science and Technology, Xiangtan, China, in 2014. He is currently working toward the M.S. degree at Hunan University, Changsha, China.

His research interests include power electronics converter technology and distributed power generation.

Shoudao Huang (M'13) was born in Hunan, China, in 1962. He received the B.S. and Ph.D. degrees from Hunan University, Changsha, China, in 1981 and 2005, respectively.

From 2008 to 2009, he was a Visiting Scholar with Aalborg University, Aalborg, Denmark. Since 2006, he has been a Professor of electrical engineering with the College of Electrical and Information Engineering, Hunan University. His interests include distributed power generation, motor driver, and control.